Simulation of Three-dimensional Convection Patterns in a Rayleigh-Benard System Using the MPS Method

Zhang, Shuai
Department of Applied Quantum Physics and Nuclear Engineering : Graduate Student

Morita, Koji
Institute of Environmental Systems : Associate Professor

Fukuda, Kenji

Shirakawa, Noriyuki
Institute of Environmental Systems : Professor

出版情報：九州大学工学紀要. 66 (1), pp.29-37, 2006-03. 九州大学大学院工学研究院
バージョン：
権利関係：

Memoirs of the Faculty of Engineering, Kyushu University, Vol.66, No.1, March 2006

Simulation of Three-dimensional Convection Patterns in a Rayleigh-Benard System Using the MPS Method

by

Shuai ZHANG[*], Koji MORITA [**], Kenji FUKUDA [***]
and Noriyuki SHIRAKAWA [†]

(Received February 6, 2006)

Abstract

The moving particle semi-implicit (MPS) method, which is a fully Lagrangian particle method, was applied to simulate the three-dimensional Rayleigh-Benard convection. The present MPS simulation reproduced typical flow patterns observed in the Rayleigh-Benard convection successfully. The results are in good agreement with those obtained by the method in the frame of the Euler system. The present results demonstrate the applicability of the MPS method to three-dimensional convective heat transfer problems.

Keywords: Moving particle semi-implicit (MPS) method, Rayleigh-Benard convection (RBC), Convection pattern

1. Introduction

The Rayleigh-Benard system is one of the representative non-equilibrium hydrodynamic systems [1)]. An adverse temperature gradient is maintained in a horizontal layer of fluid by heating the underside. On account of the thermal expansion, the fluid near the bottom will be lighter than that near the top. A stable conduction exists for this system when the temperature difference between the bottom and top boundaries is small enough. Otherwise, the static conduction becomes unstable against any small disturbance, and the system then becomes unstable.

Convection in the Rayleigh-Benard system has been extensively studied both experimentally and numerically. The earliest experiments to definitively demonstrate the Rayleigh-Benard convection were done by Benard in 1900. Rayleigh laid the theoretical foundations for this phenomenon. There have been some reviews on experiments and numerical calculations in this particular field [2)]. Recently, new technologies have been applied to investigate this phenomenon in detail, for example the molecular dynamics [3)], the direct simulation Monte Carlo [4)] and the lattice Boltzmann method [5)]. Most of these simulations were done in the Euler framework. The smoothed particle hydrodynamics (SPH) method [6)], which is a grid-free Lagrangian particle method, was used

[*] Graduate Student, Department of Applied Quantum Physics and Nuclear Engineering
[**] Associate Professor, Institute of Environmental Systems
[***] Professor, Institute of Environmental Systems
[†] Professor, Institute of Environmental Systems

to simulate the Rayleigh-Benard convection to emphasize and discuss the connection between molecular dynamics and continuum mechanics [7]. The SPH method was invented to treat with compressible flow problems. In contrast with the SPH method, a moving-particle semi-implicit (MPS) method [8], which is a deterministic Lagrangian particle method, has been developed for simulating incompressible fluids. In this method, governing equations are discretized based on particle interaction models representing gradient, Laplacian and free surface. Computational grids are unnecessary. Based on the MPS method, a combined gird and particle method, MPS-MAFL [9], has been formulated. The MPS-MAFL method has successfully simulated the natural convection in a square cavity [10]. The MPS method with a new Laplacian model and a new method for treating the boundary conditions has been used to simulate two-dimensional Rayleigh-Benard convection with a range of Rayleigh numbers [11].

Till now, most of numerical studies of the Rayleigh-Benard convection were performed for two-dimensional systems. These studies showed that the simulated critical Rayleigh number and heat flux agreed well with both theoretical results and experimental observations. However, it is also necessary to study the convection patterns by three-dimensional simulations. Watanabe obtained roll, square and hexagonal convection patterns using the direct simulation Monte Carlo method [12] and the lattice Boltzmann method [13]. In this contribution, the MPS method will be applied to simulate three-dimensional Rayleigh-Benard convection with fixed Rayleigh number and Prandtl number. Different aspect ratios will be chosen to obtain different flow patterns.

2. Numerical Models and Methods for MPS

2.1 Governing equations in MPS method

Governing equations for incompressible flows are mass, momentum and energy conservation equations as follows:

$$\frac{\partial \rho}{\partial t} + \nabla \cdot (\rho \vec{u}) = 0 \tag{1}$$

$$\frac{D\vec{u}}{Dt} = -\frac{\nabla p}{\rho} + \upsilon \nabla^2 \vec{u} + \vec{F} \tag{2}$$

$$\rho c_p \frac{DT}{Dt} = \lambda \nabla^2 T - q \tag{3}$$

2.1.1 Kernel function

In MPS, the kernel function $w(|\vec{r}_j - \vec{r}_i|, r_e)$ is chosen as [8]:

$$w(|\vec{r}_j - \vec{r}_i|, r_e) = \begin{cases} \dfrac{r_e}{(|\vec{r}_j - \vec{r}_i|)} - 1 & (|\vec{r}_j - \vec{r}_i| < r_e) \\ 0 & (|\vec{r}_j - \vec{r}_i| \geq r_e) \end{cases} \tag{4}$$

$$n^0 = \sum_{j \neq i} w(|\vec{r}_j - \vec{r}_i|, r_e) \tag{5}$$

where r_e is the cut-off radius. In the present MPS method, it is chosen to be $2.1\Delta l$, where Δl is the initial distance between two particles. With this kernel function, particle clusters can be avoided since the value of kernel function is infinity at $|\vec{r}_j - \vec{r}_i| = 0$.

2.1.2 Gradient model

Assuming two particles *i* and *j*, which possess scalar quantities Φ_i and Φ_j, respectively, the gradient in the MPS method is defined as [8]:

$$\langle \nabla \Phi \rangle_i = \frac{d}{n^0} \sum_{j \neq i} \frac{\Phi_j - \Phi_i}{\left| \vec{r}_j - \vec{r}_i \right|^2} (\vec{r}_j - \vec{r}_i) w(\left| \vec{r}_j - \vec{r}_i \right|, r_e) \tag{6}$$

where d is the number of the space dimension.

Equation (6) can be rearranged as follows:

$$\langle \nabla \Phi \rangle_i = \frac{d}{n^0} \sum_{j \neq i} \frac{\Phi_j - \Phi'_i}{\left| \vec{r}_j - \vec{r}_i \right|^2} (\vec{r}_j - \vec{r}_i) w(\left| \vec{r}_j - \vec{r}_i \right|, r_e) \tag{7}$$

where $\Phi'_i = \min(\Phi_j)$. Equation (7) is tested to be able to improve numerical stability [8].

2.1.3 Laplacian model

As we know, the Laplacian model can be derived from the divergence of gradient as

$$\langle \nabla^2 \Phi \rangle_i = \langle \nabla \cdot \nabla (\Phi)_{ij} \rangle_i \tag{8}$$

where the divergence model in the MPS method is

$$\langle \nabla \cdot \vec{\varphi} \rangle_i = \frac{d}{n^0} \sum_{j \neq i} \frac{(\vec{\varphi}_j - \vec{\varphi}_i) \cdot (\vec{r}_j - \vec{r}_i)}{\left| \vec{r}_j - \vec{r}_i \right|^2} w(\left| \vec{r}_j - \vec{r}_i \right|, r_e) \tag{9}$$

Combining the gradient model and the divergence model, we can obtain the Laplacian model [11]:

$$\langle \nabla^2 \Phi \rangle_i = \frac{2d}{n^0} \sum_{i \neq j} \frac{\Phi_j - \Phi_i}{\left| \vec{r}_j - \vec{r}_i \right|^2} w(\left| \vec{r}_j - \vec{r}_i \right|, r_e) \tag{10}$$

2.1.4 Incompressible model

In the MPS method, each particle possesses the same mass. Therefore, every particle number density n^* should be constant and equal to n^0. Otherwise, we define

$$n^* + n' = n^0 \tag{11}$$

where n' is the correction to the particle number density. The following can be derived:

$$\frac{1}{\Delta t} \frac{n'}{n^0} = -\nabla \cdot \vec{u}' \tag{12}$$

$$\vec{u}' = -\frac{\Delta t}{\rho} \nabla p^{n+1} \tag{13}$$

where $\vec{u}'$ is the velocity correction value and $n+1$ means the next time step number. As a result, we get the following pressure Poisson equation [8]:

$$\langle \nabla^2 p^{n+1} \rangle_i = -\frac{\rho}{\Delta t^2} \frac{\langle n^* \rangle_i - n^0}{n^0} \tag{14}$$

To improve calculation stability, especially for flows in an enclosure, the equation is modified as [11]:

$$\left\langle \nabla^2 p^{n+1} \right\rangle_i = \alpha_1 \frac{\rho}{\Delta t} \nabla \cdot \left\langle \vec{u}^* \right\rangle - \alpha_2 \frac{\rho}{\Delta t^2} \frac{\left\langle n^* \right\rangle_i - n^0}{n^0} \tag{15}$$

with

$$\alpha_1 + \alpha_2 = 1 \tag{16}$$

where the parameters α_1 and α_2 are chosen as 0.8 and 0.2, respectively, in the present calculations. $\vec{u}^*$ is the temporal velocity.

Equation (15) can be solved by the incomplete Cholesky conjugate gradient (ICCG) method, which is robust and fast for calculations with a large number of particles.

2.2 Time integration

The MPS method separates calculations into two stages, explicit and implicit stages, in each time step. In the explicit stage, particles move with the viscosity and external forces that are explicitly calculated by

$$\vec{u}^*{}_i = \vec{u}^n{}_i + \Delta t(\upsilon \nabla^2 \vec{u}^n{}_i + \vec{F}_i) \tag{17}$$

$$\vec{r}^*{}_i = \vec{r}^n{}_i + \Delta t \vec{u}^*{}_i \tag{18}$$

In the implicit stage, velocity is corrected with Eq. (13) to keep the conservation of the momentum equation. Time step is controlled in the computation to satisfy the following Courant condition [8]:

$$\Delta t \le 0.2 \frac{\Delta l}{u_{\max}} \tag{19}$$

where Δl is the initial distance between two particles, and $u_{\max}$ is the maximal velocity among all particles.

2.3 Boundary conditions

The original method of treating boundary conditions in MPS simulates the wall by one-layer of fixed particles with zero velocities. Other two-layer dummy particles are used for calculating the number density of the wall particles to distinguish particles on the free surface from wall particles in pressure Poisson equation. However, since the cut-off radius for both gradient and Laplacian models for the pressure Poisson equation is larger than Δl, the cut-off radius is not in agreement with the geometric boundaries. In the original MPS method, the pressure and velocity of a dummy particle is fixed as zero to solve this problem. Further, the velocities of wall and dummy particles are defined as zero to retain the non-slip boundary condition when calculating the viscosity force. However, zero velocity should be physically kept on the wall. The same difficulty will be encountered in the case of the heat transfer calculations near the wall.

To overcome such difficulties in treating boundary conditions, we define one-layer wall particles and fictitious particles that are reflected from the fluid particles by the wall, as shown in **Fig. 1**. Fluid particles interact with other fluid, wall and fictitious particles in the calculations of viscosity force and heat transfer. The fictitious particles have the same magnitude of velocities as the corresponding fluid particles, but in the opposite direction. The thermal boundary condition can be easily satisfied with this treatment. For the Dirichlet boundary condition, the average temperature of a fluid particle and the corresponding fictitious particle is kept the same as the temperature value on the wall. For the Neumann boundary condition, the temperature of the fictitious particle is the same as that of the corresponding fluid particle.

For the pressure Poisson equation, only fluid and one-layer wall particles are calculated using the ICCG method. Pressure homogeneous Neumann boundary condition is applied between

one-layer wall particles and two-layer dummy particles. **Figure 2** shows the treatment of the pressure boundary condition for the fluid particle *i*, where *j* is the wall particle that lies in the cut-off circle of particle *i*, and the particle *j'* lies at a distance of Δl in the normal direction to the wall boundary from wall particle *j*. According to the pressure Neumann boundary condition, the pressures of particles *j* and *j'* should be the same. Particle *i* will interact with particle *j'* in both the pressure gradient model and the pressure Poisson equation.

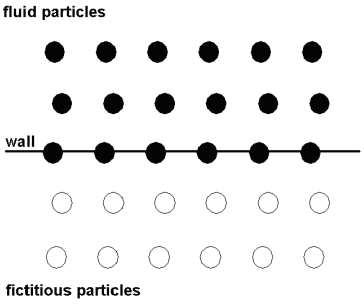

Fig. 1 Numerical treatment of thermal and velocity boundary conditions.

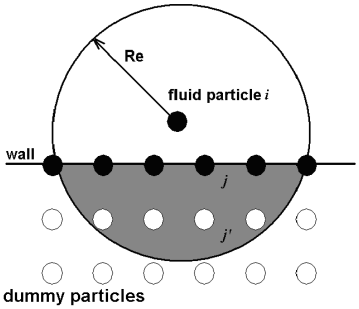

Fig. 2 Numerical treatment of pressure boundary conditions.

3. Numerical Simulations of Rayleigh-Benard Convection

3.1 Analytical model

Rayleigh-Benard convection was simulated with the Boussinesq approximation using present MPS method. The external volume force in Eq. (2) is expressed by the buoyancy force [10)]

$$\vec{F} = \beta \vec{g}(T - T_r) \tag{20}$$

where $\vec{F}$ is the acceleration due to gravity, T_r is the reference temperature that is equal to the average value of the top and bottom temperature, and β is the thermal expansion coefficient.

Figure 3 shows the geometry parameters of the Rayleigh-Benard system, where *L*, *W* and *H* are length, width and height, respectively. Periodic boundary conditions were applied in both *x* and *y* directions. The thermal and non-slip boundary conditions of upper and bottom walls were kept with fictitious particles obtained by the reflection of the fluid particles according to the walls. The value of the fictitious particle's velocity was equal to the reflected fluid particles while the direction was opposite. The temperature of the fictitious particle was chosen to keep the wall temperature constant. Fluid particles interacted with other fluid, wall and fictitious particles.

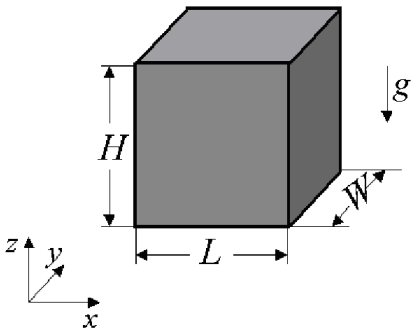

Fig. 3 Geometry parameters of the Rayleigh-Benard system.

Calculations were started from a static state except for the vertical velocity field, which was

perturbed as

$$u_z = 0.01\cos(\frac{2\pi z}{L}) \tag{21}$$

3.2 Calculation results and analysis

The MPS method has been validated to be able to estimate the critical Rayleigh number in the two-dimensional Rayleigh-Bernard simulations with the aspect ratio of 2:1 (*L*:*H*) [11]. According to the two-dimensional and three-dimensional simulations with the aspect ratio of 2:1 (*L*:*H*) and 2:2:1 (*L*:*W*:*H*), respectively, the simulated heat transfer flux agreed with a two-dimensional empirical formula with the aspect ratio of 2:1 (*L*:*H*). The roll convection pattern with the Rayleigh number and Prandtl number fixed as 6000 and 0.71, respectively, obtained by the three-dimensional simulation are shown in **Figs. 4**(a) and **5**(a).

As we know, convection patterns in the Rayleigh-Benard system are affected by several factors, such as the Rayleigh number, the Prandtl number, aspect ratio, initial disturbance and so on. A large amount of computation is necessary for studying all of these affects in detail. As a result, previous studies in this field were all concentrated on some special affect. Oscillated roll patterns were observed by increasing the Rayleigh number step by step from 6000 to 50000 with the aspect ratio of 4:4:1 (*L*:*W*:*H*) using the lattice Boltzmann method [14]. The transition between the roll to hexagonal patterns was simulated by changing the Rayleigh number near the critical value with the aspect ratio of 8:8:1 (*L*:*W*:*H*) using the direct simulation Monte Carlo method [12]. The coexistence of the roll and square patterns was numerically verified with different aspect ratios and initial disturbances using the lattice Boltzmann method [15].

All of those results were obtained in the frame of the Euler system. In the present study, the MPS method, which is a fully Lagrangian particle method, was applied to validate its capability to investigate the complicated three-dimensional Rayleigh-Bernard convection. Only the effect of the aspect ratio was considered here. Busse and Clever theoretically pointed out that it is possible to obtain stable asymmetric square convection pattern using the Galerkin method [16]. On the other hand, in Watanabe's simulations using the lattice Boltzmann method [13], the roll and square convection patterns were observed with different aspect ratios, where the Rayleigh number and Prandtl number were fixed as 5805 and 0.71, respectively. In the present simulations, the MPS method was applied to obtain the roll and square convection patterns with different aspect ratios. The number of particles in the vertical direction was chosen as 21, with which a reasonable convection pattern was obtained as shown in **Figs. 4**(a) and **5**(a) [11]. Meanwhile, the Rayleigh number and Prandtl number were fixed as 6000 and 0.71, respectively. Aspect ratio was chosen as 2:2:1, 3:3:1 and 4:4:1 (*L*:*W*:*H*).

Simulation results with different aspect ratios are compared in **Figs. 4** and **5**. **Figures 4** and **5** show the temperature contour at the middle level of the simulation region and the velocity contour in the vertical direction, respectively. In **Fig. 4**, temperature decrease is indicated by the color change from red to blue. As can be seen in **Fig. 5**, higher temperature causes lighter density, and hence causes fluid to go up. Adversely, low temperature causes fluid to go down. **Figures 4**(d) and **5**(d) indicate the roll pattern obtained with the aspect ratio of 5:5:1 as simulated with that of 2:2:1, of which results shown in **Figs. 4**(a) and **5**(a). The simulated wave numbers for the roll patterns obtained with the aspect ratios of 5:5:1 and 2:2:1 are 1 and 2, respectively. In addition, it is worth to note that the direction of these two rolls is different. The square pattern was reproduced when the aspect ratio was chosen as 4:4:1, as shown in **Figs. 4**(c) and **5**(c). In this case, the simulated wave number is 1. It seems that the square pattern occurs when two orthogonal rolls affect each other. The oscillating roll pattern with the wave number of 1.5 was observed when the aspect ratio was 3:3:1, as shown in **Figs. 4**(b) and **5**(b).

The roll and square patterns simulated with the present MPS method show a good agreement with the results obtained by the lattice Boltzmann method [13]. These results suggest that the aspect ratio affect the convection patterns since the same conditions were used for all of these four calculations except the aspect ratio. On the other hand as shown in Eq. (21), different aspect ratios

also cause different wave number in initial disturbances. Farther studies are necessary to investigate the mechanism how the aspect ratio and initial disturbance affect the convection patterns.

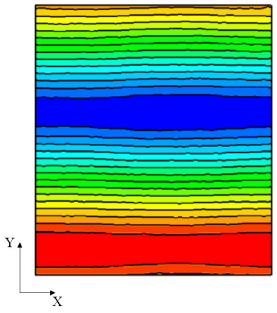

(a) 2:2:1 (particle array: 40×40×21)

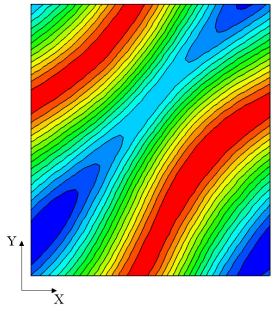

(b) 3:3:1 (particle array: 60×60×21)

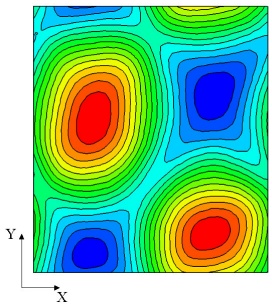

(c) 4:4:1 (particle array: 80×80×21)

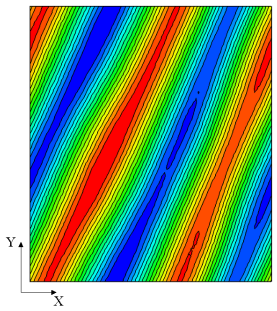

(d) 5:5:1 (particle array: 100×100×21)

Fig. 4 Temperature field at the middle elevation of the simulation region with different aspect ratios (*L*:*W*:*H*).

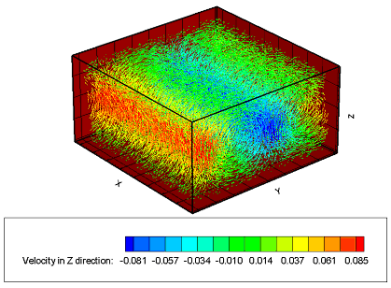

(a) 2:2:1 (particle array: 40×40×21)

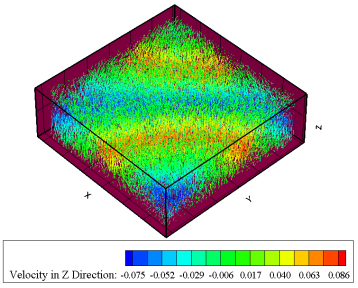

(b) 3:3:1 (particle array: 60×60×21)

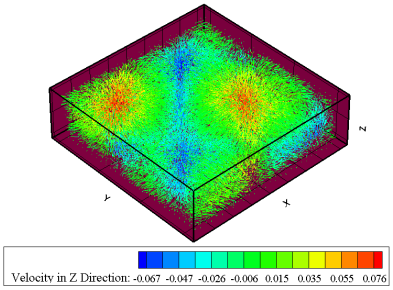

(c) 4:4:1 (particle array: 80×80×21)

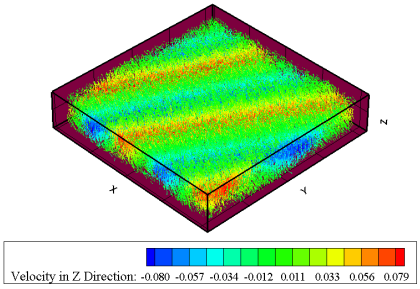

(d) 5:5:1 (particle array: 100×100×21)

Fig. 5 Three-dimensional velocity distribution and velocity contour in the vertical direction with different aspect ratios (*L*:*W*:*H*).

4. Conclusion

In this study, the MPS method was applied to the numerical simulation of flow patterns observed in Rayleigh-Benard convection systems. The results show the roll and square convection patterns, which are typical characteristics of the Rayleigh-Benard convection and are also obtained by the Euler method. The present results suggest that the MPS method is applicable to the numerical simulation of complicated three-dimensional convective heat transfer problems.

Acknowledgements

One of the authors, Shuai Zhang, gratefully acknowledges support from the Ministry of Education, Culture, Sports, Science and Technology, Japan under the MONBUKAGAKUSHO Scholarship.

Nomenclature

c_p	specific heat at constant pressure (J kg^{-1} K^{-1})
d	spatial dimensions
F	external volume force or driven force (m s^{-2})
H	height (m)
k	thermal conductivity (W m^{-1} k^{-1})
l, L	length (m)
n^0	initial number density
n^*	temporary number density
p	pressure (Pa)
q	energy transfer rate per unit volume (W m^{-3})
r	position vector (m)
Ra	Rayleigh Number
r_e	cut-off radius of the kernel function
T	temperature (K)
t	time (s)
u	velocity (m s^{-1})
v	volume (m^3)
w	kernel function
W	width (m)
Greek letters	
α_1, α_2	tuning parameters in the Poission equation
β	thermal expansion
λ	tuning parameter in the Laplacian model
φ	arbitrary vector variable
Φ	arbitrary scalar quantity
ρ	density (kg m^{-3})
υ	kinematic viscosity (m^2 s^{-1})
Δl	initial distance between two particles
Δt	time step size (s)
Subscripts	
i,j	particle number

References

1) S. Chandrasekhar; Hydrodynamic and Hydromagnetic Stability, Dover, New York, pp.9-71 (1990).

2) M.C. Cross and P.C. Hohenberg; Pattern Formation Outside of Equilibrium, Rev. Mod. Phys., Vol.65, pp.851-863 (1993).
3) M. Mareschal and E. Kestermont; Experimental Evidence for Convective Rolls in Finite Two-dimensional Molecular Models, Nature, Vol.329, pp.427-429 (1987).
4) M. El-genk and A.W. Cronenberg; An Assessment of Fuel Freezing and Drainage Phenomena in a Reactor Shield Plug Following a Core Disruptive Accident, Nucl. Eng. Des. Vol.47, No.2, pp.195-225 (1978).
5) X. He, S. Chen, et al.; A Novel Thermal Model for the Lattice Boltzmann Method in Incompressible Limit, J. Comput. Phys., Vol.146, pp.282-300 (1998).
6) L.B. Lucy; A Numerical Approach to the Testing of the Fission Hypothesis, Astron. J., Vol.82, pp.1013-1024 (1977).
7) O. Kum and W.G. Hoover; Viscous Conducting Flows with Smooth-particle Applied Mechanics, Phys. Rev. E, Vol.52, pp.4899-4908 (1995).
8) S. Koshizuka and Y. Oka; Moving-Particle Semi-implicit Method for Fragmentation of Incompressible Fluid, Nucl. Eng. Sci., Vol.123, pp.421-434 (1996).
9) H.Y. Yoon, S. Koshizuka, et al.; A particle-gridless Hybrid Method for Incompressible Flows, Int. J. Numer. Methods Fluids, Vol.30, pp.407-424 (1999).
10) S. Koshizuka, H.Y. Yoon et al.; Numerical Analysis of Natural Convection in a Square Cavity Using MPS-MAFL, Comput. Fluid Dynamics J., Vol.8, No.4, pp.485-494 (2000).
11) S. Zhang, K. Morita, et al.; An Improved MPS Method for Numerical Simulation of Convective Heat Transfer Problems, Int. J. Numer. Methods Fluids, in press.
12) T. Watanabe and H. Kaburaki; Particle Simulation of Three-dimensional Convection Patterns in a Rayleigh-Benard System, Phys. Rev. E, Vol.56, pp.1218-1221 (1997).
13) T. Watanabe; Flow Pattern and Heat Transfer Rate in Rayleigh-Benard Convection, Phys. Fluids, Vol.16, pp.972-978 (2004).
14) X. Shan; Simulation of Rayleigh-Benard Convection Using a Lattice Boltzmann Method, Phys. Rev. E, Vol.55, pp.2780-2788 (1997).
15) T. Watanabe; Numerical Evidence for Coexistence of Roll and Square Patterns in Rayleigh-Benard Convetion, Phys. Lett. A, Vol.321, pp.185-189 (2004).
16) F.H. Busse and R.M. Clever; Asymmetric Squares as an Attracting Set in Rayleigh-Benard Convection, Phys. Rev. Lett., Vol.81, pp.341-344, (1998).